Journal Name

RSCPublishing

ARTICLE

Supporting Information

MOF-directed templating synthesis of porous multicomponent dodecahedron with hollow interiors for enhanced lithium-ion battery anodes

Chencheng Sun,[a] Jun Yang,[a] Xianhong Rui,[b] Weina Zhang,[b] Qingyu Yan,[b] Peng Chen,[c] Fengwei Huo,[a] Wei Huang,*[a] and Xiaochen Dong*[a]*

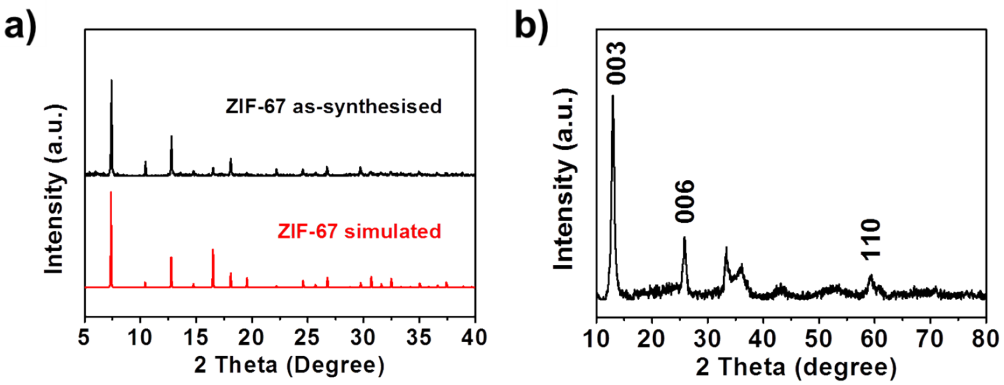

Figure S1. XRD patterns of the ZIF-67 powder (a) before and (b) after solvothermal treatment with 150 mg $Ni(NO_3)_2$.

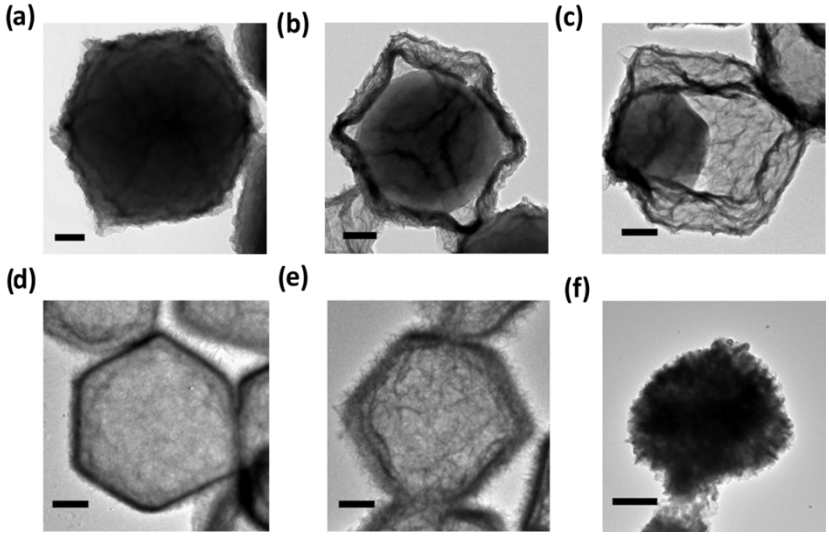

Figure S2. TEM images of the products obtained with different amount of $Ni(NO_3)_2$ at absolute ethanol for 1 h (a) 25 mg, (b) 50 mg, (c) 75 mg, (d) 100 mg, (e) 150 mg, (f) 500 mg, respectively. (all of the scale bars are 200 nm).

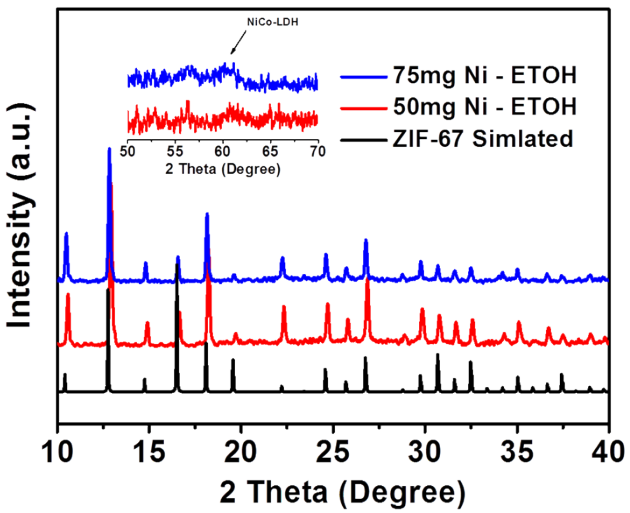

Figure S3. XRD patterns of the products obtained with 50 mg and 75 mg $Ni(NO_3)_2$ at absolute ethanol for 1 h.

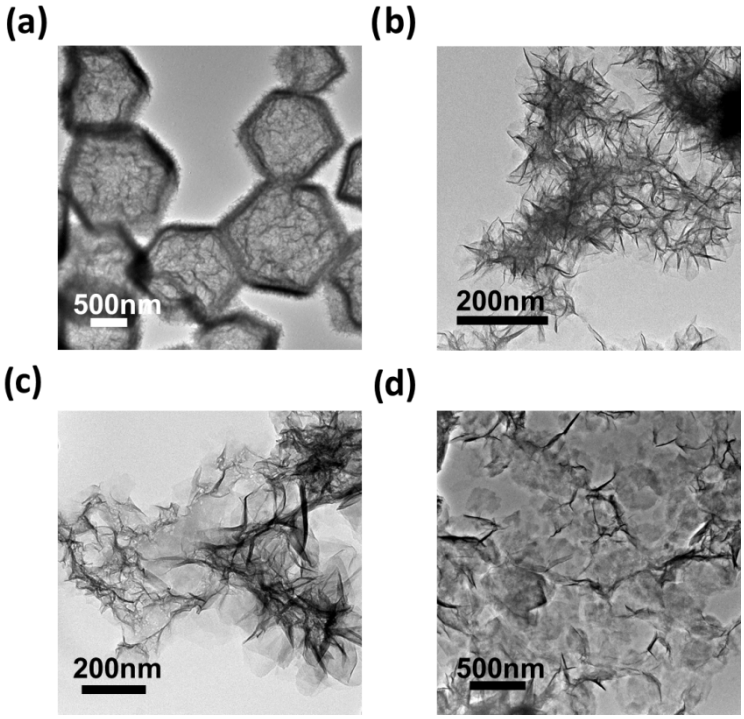

Figure S4. TEM images of the products obtained with different content of DI water in solvent at 90℃ for 1 h (a) 0, (b) 25%, (c) 50%, (d) 100%.

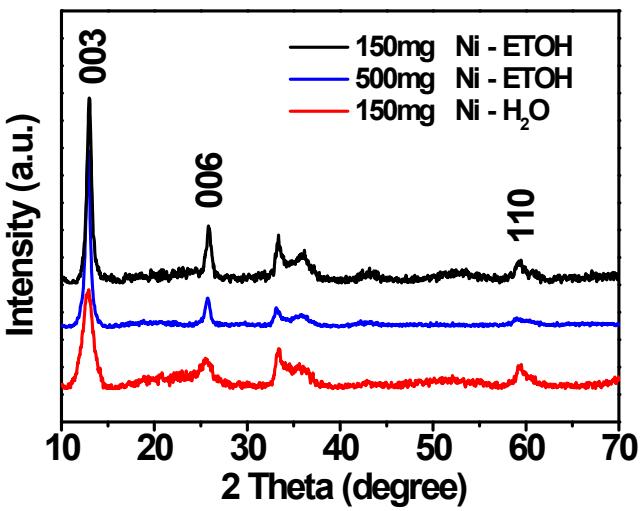

Figure S5. XRD patterns of the products obtained with various conditions. 150 mg $Ni(NO_3)_2$ at absolute ethanol (Black). 500 mg $Ni(NO_3)_2$ at absolute ethanol (Bule). 150 mg $Ni(NO_3)_2$ at DI water (Red).

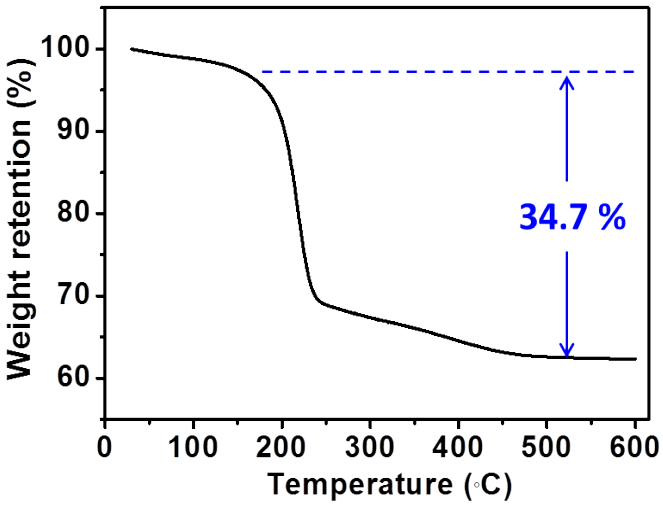

Figure S6. TGA curve of NiCo-LDH-HD obtained in the air flow at a heating rate of 2 °C min^{-1}.

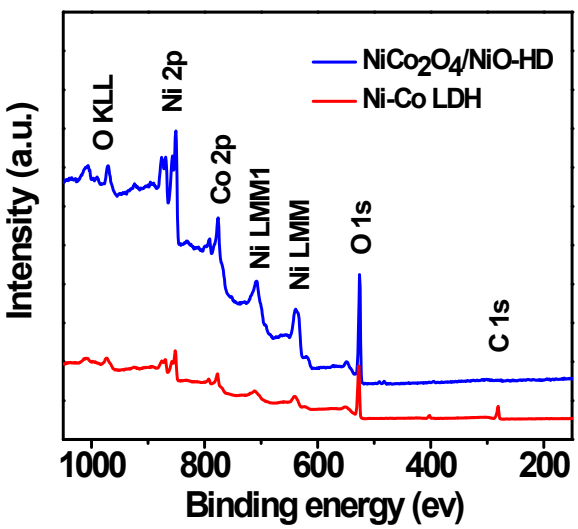

Figure S7. Survey XPS Spectra of NiCo-LDH-HD before and after calcination in air for 1h.

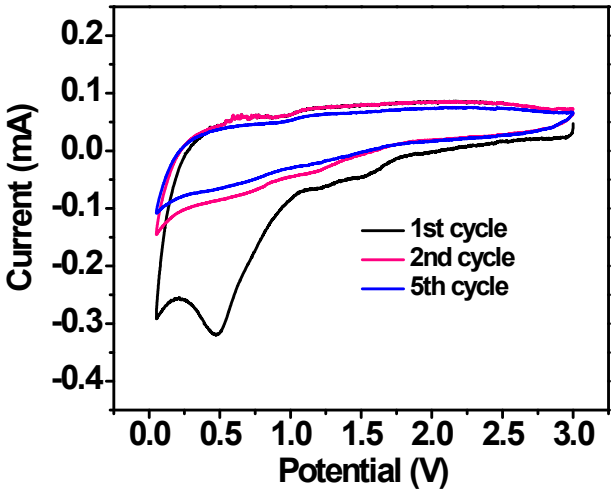

Figure S8. Representative cyclic voltammograms of ZIF-67 derived Co_3O_4 at a scan rate of 0.1 mV s^{-1} between 0.01 and 3 V *vs.* Li/Li^+.

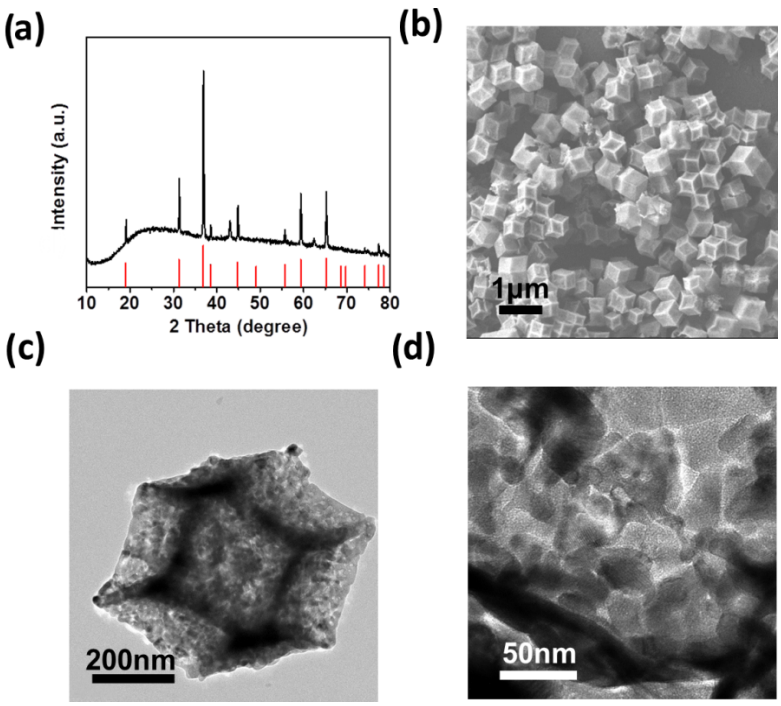

Figure S9. Characterization of CO_3O_4-HD obtained by directly calcinated ZIF-67 at air for 1h. (a) XRD pattern. (b) SEM image. (c,d) Low- and high-magnification TEM images.

Figure S10. Electrochemical impedance spectroscopy (EIS) of $NiCo_2O_4$/NiO-HD and Co_3O_4-HD electrodes.

Table S1. Comparison of electrochemical properties as the anode materials for LIBs between various cobalt-based materials and the as-synthesized porous $NiCo_2O_4$/NiO-HD in this work.

Transition metal oxide	Specific capacity (mAh g^{-1})	Current density (mA g^{-1})	Cycle stability	Reference
Co_3O_4 hollow polyhedron	~1050	100	78% (100 cycles)	1
$ZnCo_2O_4$ microsphere	975	60	98% (60 cycles)	2
$MnCo_2O_4$ microbox	827	200	75.5% (50 cycles)	3
$NiCo_2O_4$ nanosheet/rGO	1034	200	87.1% (50 cycles)	4
$CuCo_2O_4$ nanoparticle	740	60	93.4% (50 cycles)	5
$CoMoO_4$ nanoflower	1021	300	87.6% (100 cycles)	6
$Co_3O_4/CoFe_2O_4$	1354	65	~90% (60 cycles)	7
Co_3O_4/Fe_2O_3 nanowires	1200	100	82% (60 cycles)	8
$ZnO/ZnCo_2O_4$ rod arrays	978	45	92% (30 cycles)	9
$NiCo_2O_4$/NiO hollow dedocahedron	1535	200	97.3% (100 cycles)	Present work

References

1 R. Wu, X. Qian, X. Rui, H. Liu, B. Yadian, K. Zhou, J. Wei, Q. Yan, X. Q. Feng and Y. Long, Small, 2014, 10, 1932-1938.

2 Y. Sharma, N. Sharma, G. Subba Rao and B. Chowdari, Adv. Funct. Mater., 2007, 17, 2855-2861.

3 L. Zhou, D. Zhao and X. W. Lou, Adv. Mater., 2012, 24, 745-748.

4 G. Gao, H. B. Wu and X. W. D. Lou, Advanced Energy Materials, 2014.

5 Y. Sharma, N. Sharma, G. V. S. Rao and B. V. R. Chowdari, J. Power Sources, 2007, 173, 495-501.

6 H. Yu, C. Guan, X. Rui, B. Ouyang, B. Yadian, Y. Huang, H. Zhang, H. E. Hoster, H. J. Fan and Q. Yan, Nanoscale, 2014, 6, 10556-10561.

7 A. K. Rai, J. Gim, T. V. Thi, D. Ahn, S. J. Cho and J. Kim, The Journal of Physical Chemistry C, 2014, 118, 11234-11243.

8 H. Wu, M. Xu, Y. Wang and G. Zheng, Nano Research, 2013, 6, 167-173.

9 C. W. Lee, S.-D. Seo, D. W. Kim, S. Park, K. Jin, D.-W. Kim and K. S. Hong, Nano Research, 2013, 6, 348-355.